

Resonance-enhanced multiphoton-ionization–photoelectron study of the dissociative recombination and associative ionization of Xe_2^+

X. K. Hu,¹ J. B. A. Mitchell,² and R. H. Lipson^{1,*}¹*Department of Chemistry, University of Western Ontario, London, Ontario, Canada N6A 3B7*²*Physique des Atomes, Lasers, Molécules et Surfaces, UMR du CNRS No. 6627, Université de Rennes I, 35042 Rennes, France*

(Received 13 March 2000; published 13 October 2000)

Two-photon transitions from the ground state of atomic xenon gas, $\text{Xe}(^1S_0)$, to $\text{Xe}^* nf$ and np Rydberg states have been excited in an apparatus that combines ion time-of-flight and photoelectron detection capabilities. Evidence is presented that shows that xenon atoms excited to nf states with $n=4-8$ undergo rapid associative ionization with ground-state xenon atoms to form Xe_2^+ , while those excited to np states with $n=8-11$ do not. Subsequent Xe_2^+ dissociative recombination (DR) favors exit channels where xenon atoms are formed predominately in $6p$ and $5d$ excited states. Comparisons with older optical studies suggest that photoelectron spectroscopy provides a simple but effective means of studying short-time (ns) DR dynamics.

PACS number(s): 34.80.Gs, 33.60.-q, 32.10.-f, 33.15.-e

INTRODUCTION

The dissociative recombination (DR) of rare-gas dimer ions has been the subject of a number of experimental [1–17] and theoretical [18,19] studies due to their importance in laser [20] and vacuum-ultraviolet (VUV) light source [21] plasmas. The DR of Xe_2^+ ions, which, as in the case of the other rare-gas dimer systems (Ne_2^+ , Ar_2^+ , and Kr_2^+), exhibits a very large recombination rate (Table I). On the other hand, He_2^+ behaves oppositely [11] and is currently the subject of a number of experimental and theoretical studies [22–24].

Shiu *et al.* [5,6] performed a spectroscopic study of the DR process,



and identified a number of different final-state channels. In their experiments, they found that the channel leading to xenon-atom formation in $\text{Xe}^* 6p$ states dominated the reaction. However, it must be said that their method was not able to sample channels which led to the production of nonradiating metastable atoms, the ground-state channel, or other channels which produced radiation with a wavelength outside the range of detection of their spectrometer ($3800 < \lambda < 8900 \text{ \AA}$). Xenon energy levels and the strongest lines observed in fluorescence are shown schematically in Fig. 1.

Hardy and co-workers have developed a technique for identifying final product states formed in the DR of rare-gas dimer ions, which relies on a determination of their kinetic energies and so is not spectroscopically limited. They are capable, therefore, of studying recombination to metastable atom channels, though as of this time they have not examined Xe_2^+ [38].

The present paper describes an experiment where the technique of resonance-enhanced multiphoton ionization (REMPI) coupled with time-of-flight (TOF) mass spectrometry and photoelectron spectroscopy have been used to ob-

tain information concerning the relative importance of Rydberg states with different angular momenta in the process of DR and its inverse reaction, associative ionization.

EXPERIMENTAL ARRANGEMENT

The apparatus used for this study, and shown schematically in Fig. 2, can operate as either a photoionization mass spectrometer or a photoelectron spectrometer. Since both modes of operation have been described fully elsewhere [25], only the relevant details are presented here.

An $\approx 10\%$ Xe/He gas mixture, at a backing pressure of ≈ 114 psi, was introduced via a pulsed valve as a free jet into a vacuum system maintained at $\approx 10^{-6}$ Torr. The gas pulse duration was $\approx 170 \mu\text{s}$, which typically resulted in a system pressure increase to $\approx 5 \times 10^{-5}$ Torr. Although this paper is primarily concerned with atomic Xe spectroscopy, it should be appreciated that under the experimental conditions above, cold Xe_2 is also formed.

Tunable ultraviolet (UV) photons from a frequency-doubled Nd:YAG pumped dye laser operating at a 10-Hz repetition rate were focused with an $f=84$ cm quartz lens into the jet ≈ 20 mm below the nozzle pinhole to produce excited Xe atoms by resonant two-photon absorption. Laser wavelength calibration was achieved by using an Fe/Ne hollow cathode lamp to record optogalvanic Ne spectra. Two-photon excited Xe^* atoms were either subsequently ionized by (2+1) REMPI by absorbing a third photon from the same UV laser pulse, or, as shown in the next section, underwent associative ionization in certain excited states by collisions to produce Xe_2^+ . In either case, since the jet was located between the grids of a 1-m-long linear TOF mass spectrometer, the ionized species could be mass dispersed inside the TOF mass spectrometer and detected with a two-stage microchannel plate (MCP) detector.

Electrons arising from the ionization events could also be extracted in separate experiments into a double focusing electrostatic analyzer whose entrance was located 180° to the flight tube axis of the TOF mass spectrometer and horizontally ≈ 5 mm from the focus of the UV laser beam in the jet. A MCP mounted at the exit slit of the spectrometer was used

*Corresponding author. Email address: rlipson@julian.uwo.ca

TABLE I. Rate coefficients for the dissociative recombination of rare-gas dimer ions (from Ref. [19]).

Ion	Rate coefficient ($10^{-7} \text{ cm}^3 \text{ s}^{-1}$) at 300 K
He_2^+	0.0006
Ne_2^+	1.7
Ar_2^+	9.1
Kr_2^+	16
Xe_2^+	23

for detection. The kinetic-energy full width at half maximum was experimentally determined to be $\approx 170 \text{ meV}$ at 5-eV pass energy.

All MCP and optogalvanic signals were each processed in separate integrator/boxcar averagers, digitized, and stored in a computer.

RESULTS AND DISCUSSION

Figure 3 shows a composite of three (2+1) REMPI spectra for ^{132}Xe between 90 200 and 96 800 cm^{-1} . Lines involving excited-state terms with configurations $\text{Xe}^* nf[3/2]_2$, $nf[5/2]_2$, $n=4-8$, $\text{Xe}^* np[1/2]_0$, $np[3/2]_2$, and $np[5/2]_2$ with $n=8-11$ are readily observed. These states all lie above the first ionization potential for Xe_2 at 90 139.7 cm^{-1} [26].

Photoelectron spectra, obtained by (2+1) REMPI at an appropriately fixed UV laser wavelength, are shown in Figs. 4(a)–4(c) for the $\text{Xe}^* np[1/2]_0$ ($n=8,10,11$), $np[3/2]_2$, $n=9-11$, and $np[5/2]_2$, $n=9-11$ levels, respectively. The identity of the parent ion cores could be unambiguously identified by measuring the electron kinetic energies with the electron spectrometer. As illustrated schematically in Fig. 5, an atomic Xe term can display one of two separate ionization potentials corresponding to either the $^2P_{3/2}^o$ ground-state se-

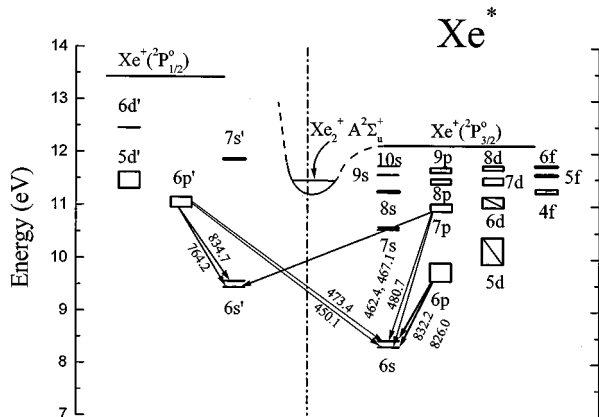


FIG. 1. Approximate partial energy-level diagram for xenon showing transitions observed by Shiu *et al.* (after Refs. [5,6]) resulting from the dissociative recombination of Xe_2^+ ions and electrons. The arrows indicate the dominant transitions observed at 300 K. The thicker arrows indicate stronger intensities. A diagonal line through a state indicates that transitions to that state were unobservable due to technical limitations.

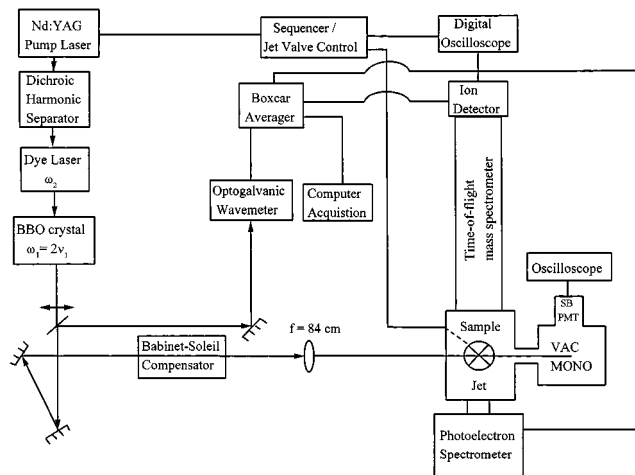


FIG. 2. Schematic diagram of the apparatus used in the present study.

ries limit at 97 834.4 cm^{-1} or the spin-orbit $^2P_{1/2}^o$ series limit at 108 371.4 cm^{-1} . The single peaks observed at relatively larger kinetic energies ($>0.5 \text{ eV}$) in most of the spectra in Fig. 4 indicate that ionization yields the ground state $^2P_{3/2}^o$ level of Xe^+ . This is in accord with published expectations [27]. The second peaks seen unexpectedly in the $\text{Xe}^* 8p[1/2]_0$ and $\text{Xe}^* 11p[1/2]_0$ spectra at lower kinetic energies ($>3.5 \text{ eV}$) due to ionization to $\text{Xe}^+ (^2P_{1/2}^o)$ may be indicative that these neutral atomic Rydberg levels suffer from interstate perturbations.

When similar REMPI photoelectron spectra were measured for the $\text{Xe}^* nf$ atomic levels, the results were found to be markedly different (Figs. 6 and 7). Here, the lines could be attributed to ionization originating from totally different, lower-energy atomic states. In particular, the dominant features arise from $\text{Xe}^* (5d)$ states, although some $\text{Xe}^* (6p)$ states do appear in certain spectra. The assignments for each spectrum are listed in Table II.

Initially, it was thought that stimulated emission down to the lower-energy Xe^* levels was the relaxation mechanism

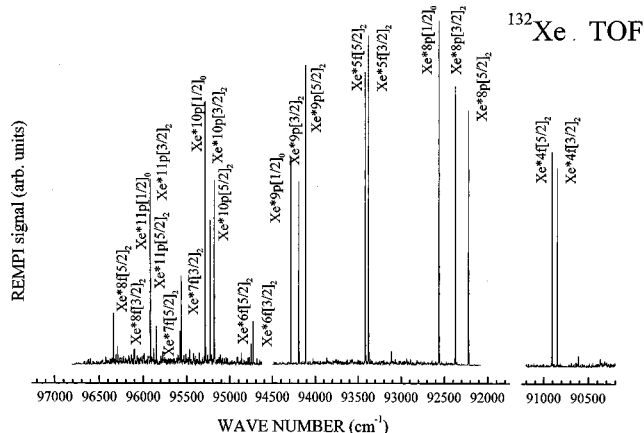


FIG. 3. A composite of three (2+1) REMPI excitation spectra recorded for the ^{132}Xe mass in the region between 90 200 and 96 800 cm^{-1} .

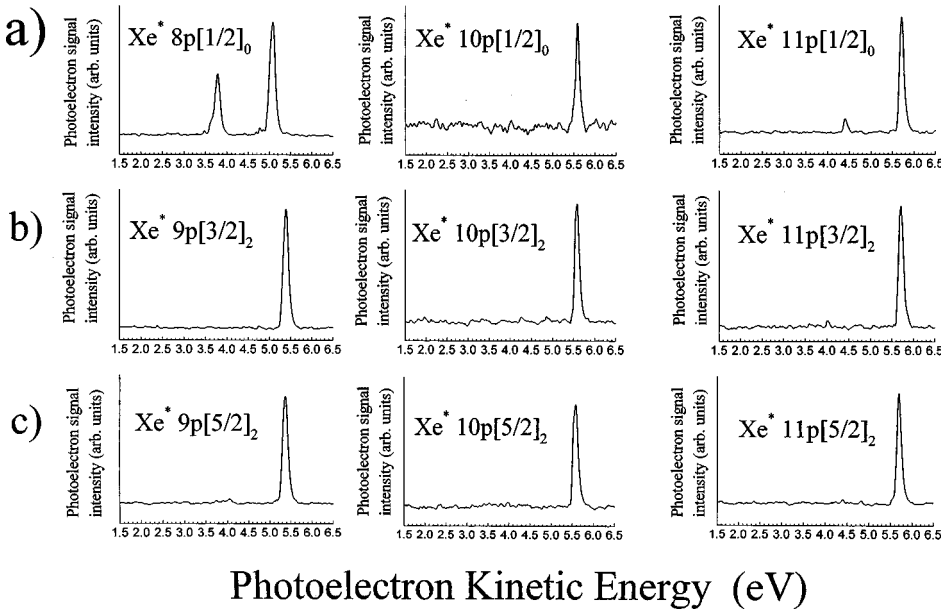
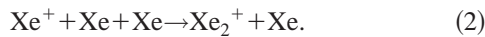


FIG. 4. REMPI photoelectron spectra recorded by exciting (a) $\text{Xe}^* np[1/2]_0$ levels, $n=8, 10,$ and 11 ; (b) $\text{Xe}^* np[3/2]_2$, $n=9-11$; and (c) $\text{Xe}^* np[5/2]_2$, $n=9-11$.

prior to ionization. Consequently, experiments were carried out to look for laser emission originating from the jet. However, such a phenomenon was ruled out as no strong emission could be observed. The answer to this surprising conundrum can be found by examining the TOF mass spectra of the ions created during these two sets of experiments. The results following excitation of the $\text{Xe}^* 5f[3/2]_2$ and $\text{Xe}^* 8p[1/2]_0$ levels, respectively, are shown in Figs. 8(a)–8(c). In both the Fig. 8(a) ($\text{Xe}^* 5f[3/2]_2 \leftarrow \text{Xe}(^1S_0)$) and Fig. 8(b) ($\text{Xe}^* 8p[1/2]_0 \leftarrow \text{Xe}(^1S_0)$) traces, the feature seen near $m/z=130$ amu corresponds to the formation of Xe^+ by (2+1) REMPI. However, in Fig. 8(a), a diffuse feature appears near $m/z=270$ amu which is attributed to the formation of Xe_2^+ . The two mass spectra were taken under free jet conditions that yielded a relatively low chamber pressure (2×10^{-5} mbar) implying a low jet density, and therefore Xe_2^+ was not believed to arise from the three-body association reaction:



Evidence for reaction (2) can be seen, however, when $\text{Xe}^* np$ states are excited under higher density free jet conditions [indicated by a higher chamber background pressure, $\geq 3 \times 10^{-5}$ mbar, Fig. 8(c)].

Further evidence for the selective formation of Xe_2^+ following excitation of $\text{Xe}^* nf$ states, but not $\text{Xe}^* np$ excitation, can be inferred from photoelectron spectra obtained by gating the electron spectrometer detection at different times. Two different kinds of photoelectrons are possible above the first ionization limit of Xe_2 . One is a near-zero-kinetic-energy electron resulting from neutral Xe_2 autoionization, while the second faster (1.5–4 eV) electron is formed by atomic Xe (2+1) REMPI (Fig. 9). Since they have different kinetic energies, the timing gates of the boxcar averager were set accordingly when recording spectra. Specifically, the fast electrons arrived at the detector ≈ 90 nsec after laser excitation, while the slower ones followed ≈ 50 nsec later. The

left-hand sides of Figs. 10(a) and 10(b) display photoelectron spectra taken via the slow electron channel. A strong, zero-energy peak is seen for the $\text{Xe}^* 5f$ excitation, which is absent from the $\text{Xe}^* 10p$ spectra. This peak arises from the ionization of excited, neutral Xe_2 molecules, which are not formed at low pressures following $\text{Xe}^* 10p$ excitation.

What is seen to be happening here is the initial formation of Xe_2^* molecules followed by autoionization to produce Xe_2^+ via the reaction [28]



This process is known as associative ionization, and gives rise to the zero-energy electron peak seen in Fig. 10 and the Xe_2^+ peak in the TOF mass spectrum in Fig. 8(a). Since the energy carried away by the electron is low, the resultant ground-state Xe_2^+ molecular ion must be left vibrationally excited. At the same time, the electron density and the time for reaction are such that the DR process

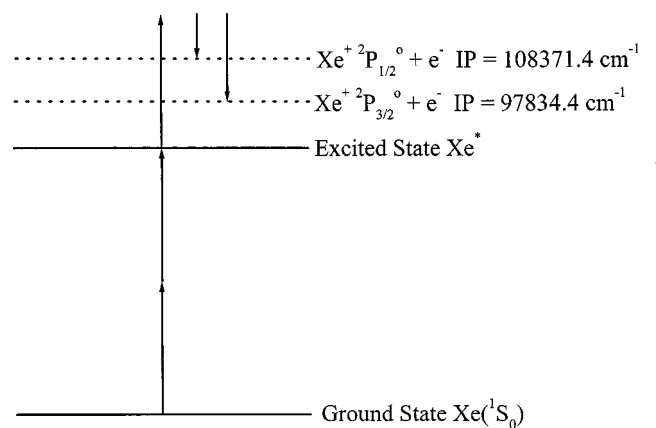


FIG. 5. A schematic energy diagram showing the excitation and ionization process for Xe^* atomic terms.

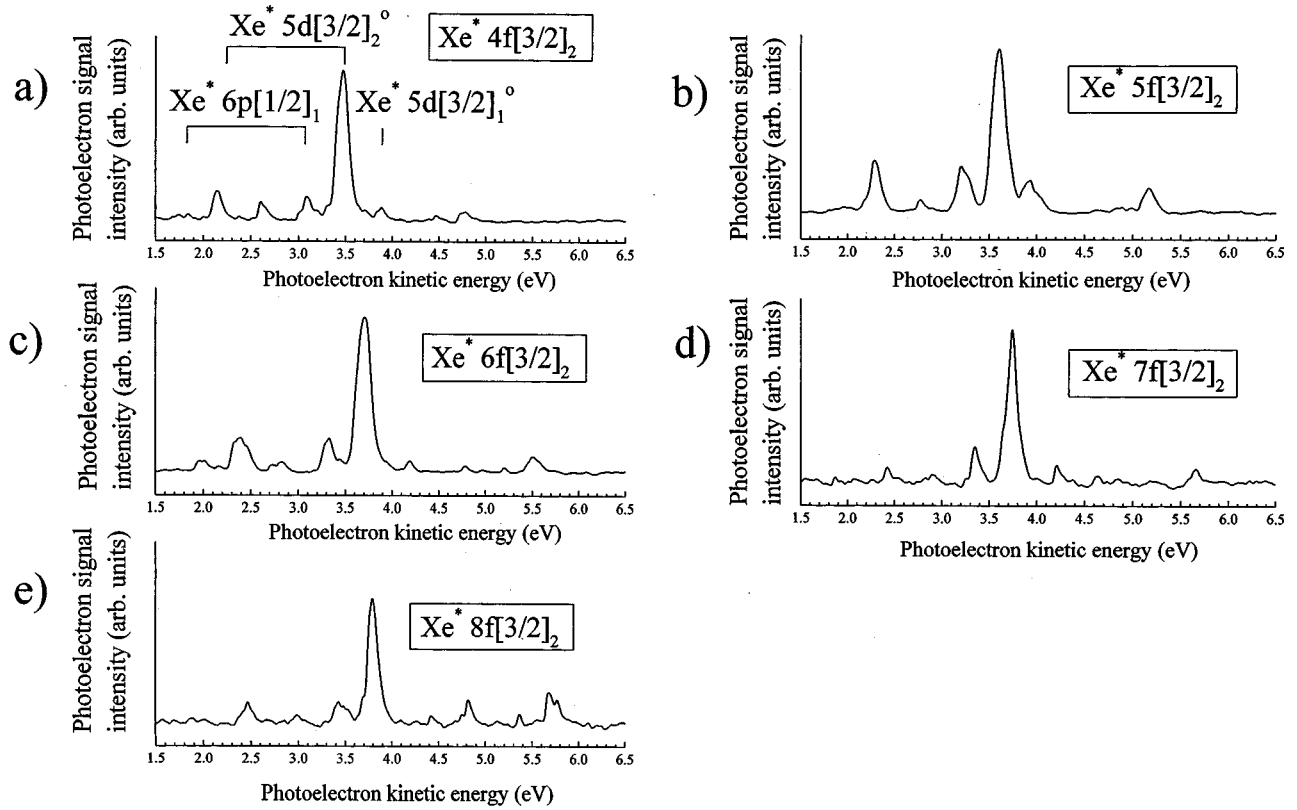


FIG. 6. REMPI photoelectron spectra recorded by exciting (a) $\text{Xe}^* 4f[3/2]_2$, (b) $\text{Xe}^* 5f[3/2]_2$, (c) $\text{Xe}^* 6f[3/2]_2$, (d) $\text{Xe}^* 7f[3/2]_2$, and (e) $\text{Xe}^* 8f[3/2]_2$ atomic terms. Dominant neutral ionization channels are indicated. The features connected by a line indicate neutral state ionization, which yields both ground-state Xe^+ spin-orbit components.

can occur, where Xe^* refers to the $\text{Xe}^* 5d$ and $\text{Xe}^* 6p$ excited states observed in Figs. 6 and 7 and listed in Table II.

To summarize these results qualitatively, associative ionization appears to proceed efficiently for $\text{Xe}^* nf$ ($n=4-8$)

atoms in collision with ground-state $\text{Xe } ^1S_0$ atoms, but much less efficiently for $\text{Xe}^* np$ ($n=8-11$) atoms under identical conditions. This means that the reverse process of DR of vibrationally excited Xe_2^+ ions with electrons tends to favor

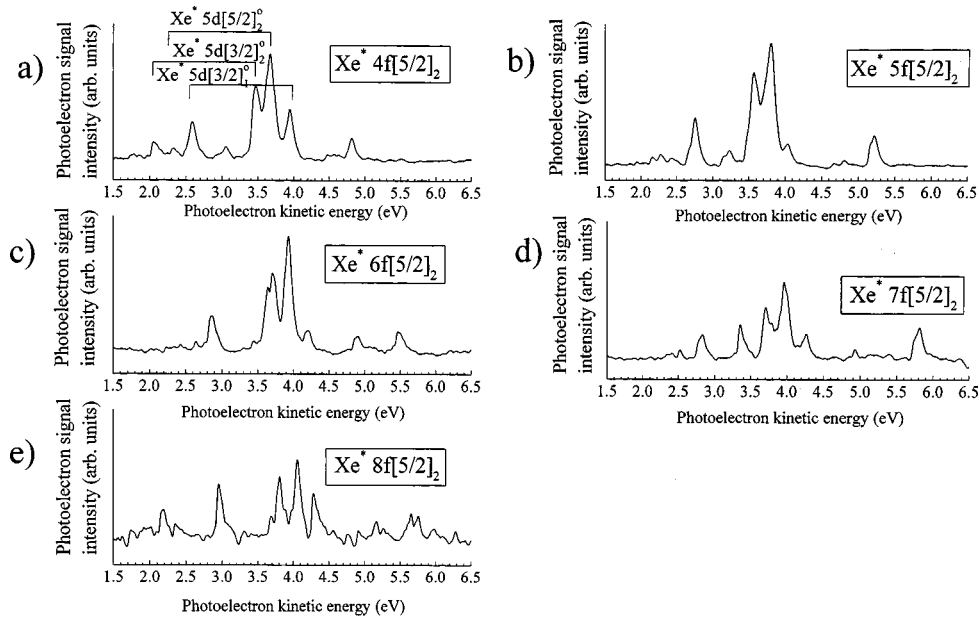


FIG. 7. REMPI photoelectron spectra recorded by exciting (a) $\text{Xe}^* 4f[5/2]_2$, (b) $\text{Xe}^* 5f[5/2]_2$, (c) $\text{Xe}^* 6f[5/2]_2$, (d) $\text{Xe}^* 7f[5/2]_2$, and (e) $\text{Xe}^* 8f[5/2]_2$ atomic terms. Dominant neutral ionization channels are indicated. The features connected by a line indicate neutral state ionization, which yields both ground-state Xe^+ spin-orbit components.

TABLE II. Kinetic energies and assignments for the recorded photoelectron peaks of the atomic levels of Xe* (4*f*–8*f*). (Peaks not determined are left blank).

Atomic state	Kinetic energy (eV)	Assignment	
Xe* 4 <i>f</i> [3/2] ₂	4.77	Xe* 4 <i>f</i> [3/2] ₂ (² P _{3/2} ^o)	
	4.52		
	3.86	Xe* 5 <i>d</i> [3/2] ₁ ^o (² P _{3/2} ^o)	
	3.47	Xe* 5 <i>d</i> [3/2] ₂ ^o (² P _{3/2} ^o)	
	3.09	Xe* 6 <i>p</i> [1/2] ₁ (² P _{3/2} ^o)	
	2.59		
	2.14	Xe* 5 <i>d</i> [3/2] ₂ ^o (² P _{1/2} ^o)	
	1.4		
	Xe* 4 <i>f</i> [5/2] ₂	4.78	Xe* 4 <i>f</i> [5/2] ₂ (² P _{3/2} ^o)
		3.93	Xe* 5 <i>d</i> [3/2] ₁ ^o (² P _{3/2} ^o)
3.67		Xe* 5 <i>d</i> [5/2] ₂ ^o (² P _{3/2} ^o)	
3.46		Xe* 5 <i>d</i> [3/2] ₂ ^o (² P _{3/2} ^o)	
3.08			
2.59		Xe* 5 <i>d</i> [3/2] ₁ ^o (² P _{1/2} ^o)	
2.35		Xe* 5 <i>d</i> [3/2] ₂ ^o (² P _{1/2} ^o)	
2.07		Xe* 5 <i>d</i> [3/2] ₂ ^o (² P _{1/2} ^o)	
Xe* 5 <i>f</i> [3/2] ₂		5.23	Xe* 5 <i>f</i> [3/2] ₂ (² P _{3/2} ^o)
	3.94	Xe* 5 <i>d</i> [5/2] ₃ ^o (² P _{3/2} ^o)	
	3.61	Xe* 5 <i>d</i> [3/2] ₂ ^o (² P _{3/2} ^o)	
	3.22	Xe* 6 <i>p</i> [1/2] ₁ (² P _{3/2} ^o)	
	2.75		
	2.29	Xe* 5 <i>d</i> [3/2] ₂ ^o (² P _{1/2} ^o)	
	1.90	Xe* 6 <i>p</i> [1/2] ₁ (² P _{1/2} ^o)	
Xe* 5 <i>f</i> [5/2] ₂	5.24	Xe* 5 <i>f</i> [3/2] ₂ (² P _{3/2} ^o)	
	4.80		
	4.07	Xe* 5 <i>d</i> [3/2] ₁ ^o (² P _{3/2} ^o)	
	3.81	Xe* 5 <i>d</i> [5/2] ₂ ^o (² P _{3/2} ^o)	
	3.59	Xe* 5 <i>d</i> [3/2] ₂ ^o (² P _{3/2} ^o)	
	3.20		
	2.75	Xe* 5 <i>d</i> [3/2] ₁ ^o (² P _{1/2} ^o)	
	2.28	Xe* 5 <i>d</i> [3/2] ₂ ^o (² P _{1/2} ^o)	
	Xe* 6 <i>f</i> [3/2] ₂	5.49	Xe* 6 <i>f</i> [3/2] ₂ (² P _{3/2} ^o)
5.19			
4.75			
4.21		Xe* 5 <i>d</i> [3/2] ₁ ^o (² P _{3/2} ^o)	
3.70		Xe* 5 <i>d</i> [3/2] ₂ ^o (² P _{3/2} ^o)	
3.32		Xe* 6 <i>p</i> [1/2] ₂ (² P _{3/2} ^o)	
2.82			
2.38	Xe* 5 <i>d</i> [3/2] ₂ ^o (² P _{1/2} ^o)		
2.01	Xe* 6 <i>p</i> [1/2] ₁ (² P _{1/2} ^o)		
Xe* 6 <i>f</i> [5/2] ₂	5.49	Xe* 6 <i>f</i> [5/2] ₂ (² P _{3/2} ^o)	
	4.94		
	4.19	Xe* 5 <i>d</i> [3/2] ₁ ^o (² P _{3/2} ^o)	
	3.92	Xe* 5 <i>d</i> [5/2] ₂ ^o (² P _{3/2} ^o)	
	3.69	Xe* 5 <i>d</i> [3/2] ₂ ^o (² P _{3/2} ^o)	
	2.86	Xe* 5 <i>d</i> [3/2] ₁ ^o (² P _{1/2} ^o)	
Xe* 7 <i>f</i> [3/2] ₂	5.64	Xe* 7 <i>f</i> [3/2] ₂ (² P _{3/2} ^o)	
	4.18	Xe* 5 <i>d</i> [3/2] ₁ ^o (² P _{3/2} ^o)	

TABLE II. (Continued).

Atomic state	Kinetic energy (eV)	Assignment
	3.74	Xe* 5 <i>d</i> [3/2] ₂ ^o (² P _{3/2} ^o)
	3.35	Xe* 6 <i>p</i> [1/2] ₁ (² P _{3/2} ^o)
	2.42	Xe* 5 <i>d</i> [3/2] ₂ ^o (² P _{1/2} ^o)
Xe* 7 <i>f</i> [5/2] ₂	5.65	Xe* 7 <i>f</i> [5/2] ₂ (² P _{3/2} ^o)
	4.82	
	4.20	Xe* 5 <i>d</i> [3/2] ₁ ^o (² P _{3/2} ^o)
	3.96	Xe* 5 <i>d</i> [5/2] ₂ ^o (² P _{3/2} ^o)
	3.74	Xe* 5 <i>d</i> [3/2] ₂ ^o (² P _{3/2} ^o)
	3.35	Xe* 6 <i>p</i> [1/2] ₁ (² P _{3/2} ^o)
	2.88	Xe* 5 <i>d</i> [3/2] ₁ ^o (² P _{1/2} ^o)
Xe* 8 <i>f</i> [3/2] ₂	5.74	Xe* 8 <i>f</i> [3/2] ₂ (² P _{3/2} ^o)
	4.82	
	4.46	
	3.79	Xe* 5 <i>d</i> [3/2] ₂ ^o (² P _{3/2} ^o)
	3.42	Xe* 6 <i>p</i> [1/2] ₁ (² P _{3/2} ^o)
	2.94	
Xe* 8 <i>f</i> [5/2] ₂	2.46	Xe* 5 <i>d</i> [3/2] ₂ ^o (² P _{1/2} ^o)
	5.74	Xe* 8 <i>f</i> [5/2] ₂ (² P _{3/2} ^o)
	5.20	
	4.28	Xe* 5 <i>d</i> [3/2] ₁ ^o (² P _{3/2} ^o)
	4.06	Xe* 5 <i>d</i> [5/2] ₂ ^o (² P _{3/2} ^o)
	3.82	Xe* 5 <i>d</i> [3/2] ₂ ^o (² P _{3/2} ^o)
	2.95	
	2.15	

the formation of Xe* *nf* (*n* = 4–8) final states over Xe* *np* (*n* = 8–11). At this time a quantitative explanation cannot be offered for this striking difference. One possible reason that was considered is a simple orbital size effect. The mean ra-

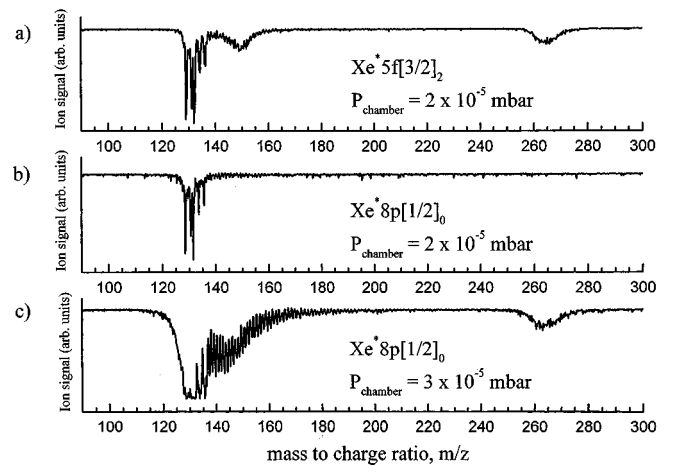


FIG. 8. Time-of-flight mass spectra obtained by exciting the (a) Xe* 5*f*[3/2]₂ and (b) Xe* 8*p*[1/2]₀ atomic levels under identical experimental conditions. (Chamber pressure 2×10^{-5} mbar.) (c) Time-of-flight mass spectra obtained by exciting the Xe* 8*p*[1/2]₀ atomic level under conditions with a higher background chamber pressure (3×10^{-5} mbar). In this case it is then possible to see weak associative ionization occurring.

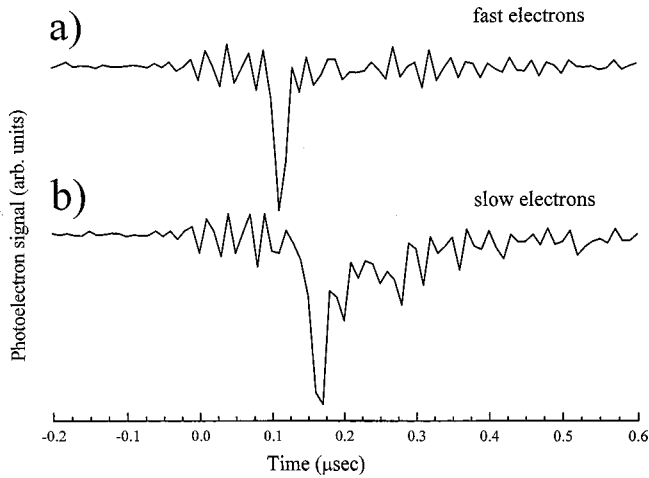


FIG. 9. (a) Time-of-flight mass spectra gated for the arrival of (a) fast photoelectrons produced by REMPI and (b) slow photoelectrons produced by Xe_2 autoionization.

dius of a particular Xe^* atom was estimated using the following hydrogeniclike equation [29]:

$$\langle r_{n^*,l} \rangle = \frac{n^{*2}}{z} \left\{ 1 + \frac{1}{2} \left[1 - \frac{l(l-1)}{n^{*2}} \right] \right\} a_0, \quad (5)$$

where z is the charge of the ion core, l is the orbital angular momentum, and a_0 is the Bohr radius. The effective principle quantum number, n^* , is equal to $n - \delta$, where δ is the quantum defect. If the resonant Xe atomic level frequency, ν , and the ionization potential of the atom, V_{ion} , are known [27], n^* can be calculated from the well-known Rydberg formula

$$\nu = V_{\text{ion}} - \frac{\mathcal{R}}{n^{*2}}. \quad (6)$$

Here \mathcal{R} is the Rydberg constant.

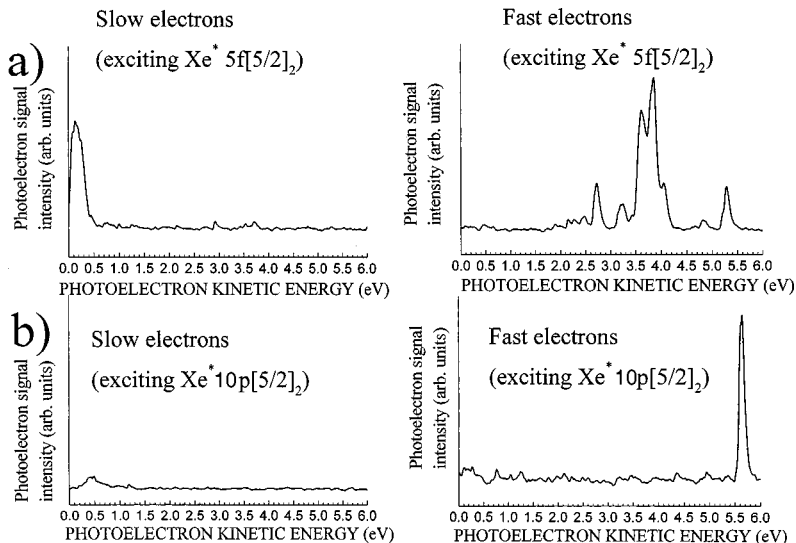


FIG. 10. (a) Left-hand side: photoelectron spectra recorded by exciting $\text{Xe}^* 5f[5/2]_2$, which shows the relatively large approximately zero kinetic-energy peak obtained gating for slow electrons; right-hand side: photoelectron spectra obtained by exciting $\text{Xe}^* 5f[5/2]_2$ and gating for fast electrons. (b) Left-hand side: photoelectron spectra recorded by exciting $\text{Xe}^* 10p[5/2]_2$, which shows the relatively small approximately zero kinetic-energy peak obtained gating for slow electrons; right-hand side: photoelectron spectra obtained by exciting $\text{Xe}^* 10p[5/2]_2$ and gating for fast electrons.

Calculations show, for example, that the mean radius for $\text{Xe}^* 11p[3/2]_2$ is 43.9 Å, which is approximately four times larger than the mean radius of $\text{Xe}^* 4f[3/2]_2$ (9.26 Å). Moreover, when N_2 gas was introduced in the gas mixture to minimize the number of collisions between Xe atoms by simple dilution, Xe_2^+ signals were still strongly detected. Hence it was concluded that orbital size is not a dominant criterion.

In Shiu *et al.*'s experiment [5,6], it was observed that the lower-energy $\text{Xe}^* np$ states (and in particular the $\text{Xe}^* 6p$ states) were the dominant final channel for DR. In fact, this channel has also been identified in this work as having a contribution to the process, as seen in Table II. The major channel leading to $\text{Xe}^* 5d$ is, however, more often seen in this work, and so may be more favored than the formation of $\text{Xe}^* 6p$. The $\text{Xe}^* 5d$ channel could not be seen in the earlier experiments due to spectroscopic limitations, and so its importance could not be accounted for. In other measurements concerning the recombination of the rare-gas molecular ions Ne_2^+ , Ar_2^+ , and Kr_2^+ , Hardy and co-workers [14–17] have identified channels forming $(n+1)s$ states in Ne, Ar, and Kr, $n=2,3,4$ as being major products of DR. Such states were also not detected in Shiu *et al.*'s experiment since, being metastable, they do not radiate after formation.

An examination of the crude potential energy curves for Xe_2^+ and Xe_2 in Refs. [30] and [31] indicates that states dissociating to the $\text{Xe} + \text{Xe}^* 6p$ pass close to the minimum of the potential well of Xe_2^+ and thus could be a major channel for direct DR. Dimer states dissociating to $\text{Xe} + \text{Xe}^* 5d$ must lie quite close to these levels, and therefore intersect the Xe_2^+ ground state in the vicinity of its lower vibrationally excited levels. Due to a lack of information on the position and the shapes of the potential energy curves of the dimer Rydberg states dissociating to higher $\text{Xe}^* n$ states, and in particular for those states that are participating in associative ionization, we cannot comment on why f states should be favored over p states in this region. This would seem to be a question of intrinsic interest to the theory of DR and to the modeling of dynamical effects in the dissociation of high molecular Rydberg states. It certainly appears that curve

crossings in this region favor an exit trajectory toward the f states rather than the p states. This conclusion could not be gleaned from earlier and slower (μs time scale) optically based DR studies, and therefore our results demonstrate that dispersive photoelectron spectroscopy provides a powerful method to sample the short-time (ns time scale) dynamics in this regard.

Another question that should be addressed with respect to Xe_2^+ DR is the reason for the very high thermal rate coefficient ($23 \times 10^{-7} \text{ cm}^3 \text{ s}^{-1}$), which is an order of magnitude greater than rates for lighter diatomic ions such as O_2^+ . Bates [19] has attempted to explain this in terms of it being an example of super-dissociative-recombination. This is a phenomenon where the recombination proceeds to high Rydberg states so that the gradient of the crossing state is shallow, leading to a very good Franck-Condon overlap between the initial ion state and the intermediate molecular state. Super-DR has been demonstrated for a number of experiments concerning the recombination of high vibrational levels of H_2^+ [32–34]. The fact that our results and others show that, for the case of Xe_2^+ DR, lower states are favored over high Rydberg states perhaps weakens the argument that super-DR is responsible for the large rate.

CONCLUSIONS

The experiment described in this paper demonstrates a method for obtaining state-specific information concerning the associative ionization and dissociative recombination of rare-gas dimer ions. This type of information is very necessary for modeling light source plasmas [35] and plasma display panels [36,37]. In future studies, we intend to examine similar processes in neon, argon, and krypton gases, as well as rare-gas mixtures.

ACKNOWLEDGMENTS

This work was supported by the Natural Sciences and Engineering Research Council of Canada, and the University of Western Ontario. The authors thank Professor D. W. Setser for valuable suggestions. X. K. H. is grateful to the Ontario government for financial support. R. H. L. would like to thank CNRS for financial support at the University of Rennes.

-
- [1] F. J. Mehr and M. A. Biondi, *Phys. Rev.* **176**, 322 (1968).
 [2] L. Frommhold and M. A. Biondi, *Phys. Rev.* **185**, 244 (1969).
 [3] J. Philbrick, F. J. Mehr, and M. A. Biondi, *Phys. Rev.* **181**, 271 (1969).
 [4] Y.-J. Shiu and M. A. Biondi, *Phys. Rev. A* **16**, 1817 (1977).
 [5] Y.-J. Shiu, M. A. Biondi, and D. P. Sipler, *Phys. Rev. A* **15**, 494 (1977).
 [6] Y.-J. Shiu and M. A. Biondi, *Phys. Rev. A* **17**, 868 (1978).
 [7] A. J. Cunningham and R. M. Hobson, *Phys. Rev.* **185**, 98 (1969).
 [8] A. J. Cunningham and R. M. Hobson, *J. Phys. B* **5**, 1773 (1972).
 [9] J. N. Fox and R. M. Hobson, *Phys. Rev. Lett.* **17**, 161 (1966).
 [10] H. J. Oskam and V. R. Mittelstadt, *Phys. Rev.* **132**, 1445 (1963).
 [11] H. J. Oskam, in *Case Studies in Atomic Collision Physics I*, edited by E. W. McDaniel and M. R. C. McDowell (North-Holland, Amsterdam, 1969), p. 465.
 [12] L. Mikus, *J. Phys. D* **11**, L39 (1978).
 [13] L. Malinovsky, P. Lukac, J. Trnovec, C. J. Hong, and A. Talsky, *Czech. J. Phys.* **40**, 191 (1990).
 [14] G. B. Ramos, M. Schlamkowitz, J. Sheldon, K. A. Hardy, and J. R. Peterson, *Phys. Rev. A* **51**, 2945 (1995).
 [15] G. Ramos, G. J. W. Sheldon, K. A. Hardy, and J. R. Peterson, *Phys. Rev. A* **56**, 1913 (1997).
 [16] A. Barrios, J. W. Sheldon, K. A. Hardy, and J. R. Peterson, *Phys. Rev. Lett.* **69**, 1348 (1992).
 [17] G. B. Ramos, M. Schlamkowitz, J. Sheldon, K. Hardy, and J. R. Peterson, *Phys. Rev. A* **52**, 4556 (1995).
 [18] T. F. O'Malley, *Phys. Rev.* **185**, 101 (1969).
 [19] D. R. Bates, *J. Phys. B* **24**, 703 (1991).
 [20] G. J. Volkova, *Opt. Technol.* **64**, 637 (1997).
 [21] G. Volkova and G. Gerasimov, *Quantum Electron.* **27**, 213 (1997).
 [22] X. Urbain, in *Dissociative Recombination: Theory, Experiment and Application IV*, edited by M. Larsson, J. B. A. Mitchell, and I. Schneider (World Scientific, Singapore, 1999), p. 16.
 [23] X. Urbain, C. P. Safvan, M. J. Jensen, and L. H. Andersen, in *Dissociative Recombination: Theory, Experiment and Application IV* (Ref. [22]), p. 261.
 [24] L. Carata, A. Larsson, A. E. Orel, and A. Suzor-Weiner, in *Dissociative Recombination: Theory, Experiment and Application IV* (Ref. [22]), p. 289.
 [25] S. S. Dimov, R. H. Lipson, T. Turgeon, J. A. Vanstone, and D. S. Wang, *J. Chem. Phys.* **100**, 8666 (1994); S. S. Dimov, J. Y. Cai, and R. H. Lipson, *ibid.* **101**, 10 313 (1994); X. K. Hu, D. M. Mao, S. S. Dimov, and R. H. Lipson, *Phys. Rev. A* **54**, 2814 (1996).
 [26] R. I. Hall, Y. Lu, Y. Morioka, T. Matsui, T. Tanaka, H. Yoshii, T. Hayaishi, and K. Ito, *J. Phys. B* **28**, 2435 (1995).
 [27] C. E. Moore, *Atomic Energy Levels*, Natl. Bur. Stand. (U.S.) Circ. No. 467 (U.S. GPO, Washington, DC, 1971), Vol. III.
 [28] S. T. Pratt, P. M. Dehmer, and J. L. Dehmer, *Chem. Phys. Lett.* **165**, 131 (1990).
 [29] H. Lefebvre-Brion and R. W. Field, *Perturbations in the Spectra of Diatomic Molecules* (Academic, Orlando, 1986).
 [30] N. Bowering, M. R. Bruce, and J. W. Keto, *J. Chem. Phys.* **84**, 709 (1986).
 [31] R. S. Mulliken, *J. Chem. Phys.* **52**, 5170 (1970).
 [32] J. B. A. Mitchell, F. B. Yousif, P. J. T. van der Donk, T. J. Morgan, and M. I. Chibisov, *Int. J. Mass Spectrom. Ion Processes* **149/150**, 153 (1995).
 [33] M. I. Chibisov, J. B. A. Mitchell, P. J. T. Van der Donk, F. B.

- Yousif, and T. J. Morgan, Phys. Rev. A **56**, 443 (1997).
- [34] W. van der Zande, J. Semaniak, V. Zengin, G. Sundström, S. Rosén, C. Strömholm, S. Datz, H. Danared, and M. Larsson, Phys. Rev. A **54**, 5010 (1996).
- [35] G. Gerasimov and G. Zvereva, in *Dissociative Recombination: Theory, Experiment and Application IV* (Ref. [22]), p. 275.
- [36] S. Rauf and M. J. Kushner, J. Appl. Phys. **85**, 3460 (1999).
- [37] T. van der Stratten and M. J. Kushner, J. Appl. Phys. **87**, 2700 (2000).
- [38] K. Hardy (private communication).